Research Square

Preprints are preliminary reports that have not undergone peer review.
They should not be considered conclusive, used to inform clinical practice,
or referenced by the media as validated information.

Design and Preliminary Prototype Evaluation of a Low- Cost IoT-Enabled Stair-Climbing Wheelchair

Ghada A. Elgamal

Ghada.a.elgamal@gmail.com

Egyptian Chinese University

Nerveen Ehab

University of Hertfordshire by GAF

A. M. Bassiuny

Faculty of Engineering, Capital University (formerly Helwan University)

Research Article

Keywords: stair-climbing wheelchair, assistive technology, IoT, BLDC hub motor, linear actuator, static stability, failure analysis, NodeMCU ESP8266

Posted Date: November 11th, 2026

DOI: https://doi.org/10.21203/rs.3.rs-11413767/v1

License: This work is licensed under a Creative Commons Attribution 4.0 International License.
Read Full License

Additional Declarations: No competing interests reported.

Design and Preliminary Prototype Evaluation of a Low-Cost IoT-Enabled Stair-Climbing Wheelchair

Ghada A. Elgamal[1]*, Nerveen Ehab[2], A.M. Bassiuny[3,4]

[1] *Mechatronics Engineering Department, Faculty of Engineering and Technology, Egyptian Chinese University, Cairo, Egypt*

[2] *Mechanical Engineering and Mechatronics, University of Hertfordshire by GAF, Cairo, Egypt*

[3] *Mechanical Engineering Department, Faculty of Engineering, Capital University (formerly Helwan University), Cairo, Egypt*

[4] *Higher Technology Institute, New Heliopolis, Cairo, Egypt*

**** Corresponding Author: Ghada.a.elgamal@gmail.com | ghada.abdelzaher@ecu.edu.eg***

ABSTRACT

This paper reports a preliminary laboratory evaluation of a low-cost stair-climbing wheelchair prototype and identifies the mechanical limits that govern its failures under load on a representative Egyptian residential staircase. The prototype, a smart stair-climbing wheelchair (SCW), combines a rear motorized stair-tread mechanism actuated by two 12 V linear actuators, differential-drive 24 V brushless hub motors, and a NodeMCU ESP8266 control and IoT layer providing Blynk-based remote override, GPS tracking and infrared obstacle detection for level-ground driving. Analytical models of actuator kinematics, actuator force, drive torque, power budget, traction and static stability were developed and compared with measurements. On a five-step laboratory staircase (riser 175 mm, tread 275 mm, pitch 32.5°), the prototype completed 10 of 10 unloaded ascents (100%; exact 95% CI 69–100%) and 7 of 10 ascents with a 70 kg dead-weight load (70%; 95% CI 35–93%). All loaded failures occurred at the terminal-step transition; tread slip was the recorded failure mode in all three cases, and the models attribute it to a combination of insufficient drive-torque margin (≈83 N·m demand per motor versus a 45 N·m continuous and an 85 N·m peak rating) and marginal tread traction (required friction coefficient 0.64 versus ≈0.65 available). For the 100 kg design payload (130 kg total mass) the models predict ≈106 N·m per motor, above the peak rating, and an actuator safety factor of only 1.33, and the preliminary static-stability estimate indicates that the chair is not self-stable on the flight without attendant support. The measured actuator extension (92 ± 3 mm) and the current-based peak torque estimate (83 N·m) were consistent with the model predictions within 5%. The IoT layer achieved a mean remote-command latency of 180 ms, an obstacle-stop latency of 45 ms and a GPS accuracy of 2.5–3.5 m, at a prototype component cost of USD 350–450. The results demonstrate the feasibility of the low-cost architecture but not yet its reliability for users; specific design corrections and a validation plan are proposed. No human participants were involved, and the findings do not constitute clinical validation.

Keywords: *stair-climbing wheelchair; assistive technology; IoT; BLDC hub motor; linear actuator; static stability; failure analysis; NodeMCU ESP8266*

NOMENCLATURE

Symbol	Description	Unit / Value	Symbol	Description	Unit / Value
θ_{stair}	Staircase inclination angle	degrees	r_w	Drive wheel radius	m
H_r	Stair riser height	mm	T_{motor}	Motor torque requirement per hub	N·m
D_t	Stair tread depth	mm	P_{total}	System power draw at rated motor power	W
ΔL	Required linear actuator extension	mm	I_{peak}	Battery current at rated motor power	A
L_{arm}	Actuator pivot moment arm	mm	C_{Ah}	Battery nominal capacity	Ah

M	Total system mass (chair + occupant)	kg	V_{right}- V_{left}	Differential PWM speed commands	–
F_p	Required propulsive force at wheel rim	N	k	Joystick ADC-to-PWM scaling constant	$PWM_{max}/511$
μ_r	Rolling resistance coefficient	~0.02	V_{batt}	Battery nominal voltage (8S $LiFePO_4$)	V (25.6)
F_{act}	Force per linear actuator	N	I_{charge}	Charging current	A
d_A	Perpendicular distance, pivot O to actuator line of action	mm	η_{charge}, η_{DC}	Charging efficiency; DC–DC converter efficiency	–
d_W	Lever arm of tread load about pivot O	mm	PWM_{max}	Maximum PWM command value	–
λ	Share of total weight carried by the tread assemblies	–	μ_{req}, μ_s	Required and available (literature) static friction coefficient (tread/nosing)	–
a, b, φ_0	Actuator anchor distances |OA|, |OB| and initial angle AOB	mm, mm, °	β	Static stability margin angle	degrees
x_G, z_G	CoG position relative to rear support contact (parallel / normal to support line)	mm	E	Usable battery energy	Wh
T_{peak}, K_t	Motor peak torque; torque constant	N·m; N·m/A	P_{avg}	Average battery power	W

1. INTRODUCTION

Mobility impairment is a major contributor to functional disability worldwide. An estimated 1.3 billion people, about 16% of the global population, experience significant disability [1], and approximately 2.5 billion people need at least one assistive product [2]. For users of electric-powered wheelchairs, staircases, elevated thresholds and the absence of ramps or lifts remain the most immediate physical barriers to independent mobility [3].

The problem is particularly acute in lower- and middle-income settings, where access to assistive technology is limited by cost, supply and maintenance capacity [2,4], and where retrofitting existing residential buildings with ramps or lifts is often impractical. In Greater Cairo, persons with disabilities continue to report substantial physical barriers in public places, including stairs and inaccessible entrances [5].

Stair-climbing wheelchairs address this problem by adapting the device to the existing environment rather than the environment to the device. Established approaches include wheel-cluster mechanisms [6–8], legged and leg–wheel hybrid mechanisms [9–11], tracked crawlers [3,12,13] and dynamically balancing platforms such as the iBOT [14]; their trade-offs among autonomy, stability, complexity and cost have been reviewed in [3,15]. Commercial devices nevertheless remain expensive relative to incomes in developing regions, and clinical evaluation has shown that reliability and perceived safety during stair negotiation are decisive for user acceptance [16].

In parallel, low-cost Wi-Fi microcontrollers and cloud platforms have made it feasible to add remote monitoring, location tracking and remote override to powered wheelchairs [17–21], and remote-monitoring architectures developed for other mechatronic systems provide transferable design patterns [22]. Such functions are potentially most valuable during stair negotiation, the highest-risk phase of use; however, IoT functions and stair-climbing mechanisms have largely been developed separately, and low-cost prototypes combining them have rarely been reported together with quantitative stair-climbing data.

The present work reports the design, fabrication and preliminary laboratory evaluation of a Smart Climbing Wheelchair (SCW) that combines a rear-mounted motorized stair-tread mechanism actuated by two linear actuators, BLDC hub-motor differential drive, joystick control, and a NodeMCU ESP8266 IoT layer (Blynk remote override, GPS tracking and infrared obstacle detection for level-ground driving), all built from commercially

available components. The study addresses the following engineering research question: can a low-cost stair-tread mechanism driven by 250 W commercial hub motors negotiate a representative Egyptian residential staircase (riser 175 mm, tread 275 mm) under an occupant-equivalent load, and which mechanical limit (drive torque, tread traction or static stability at the terminal step) governs its failures? The question is addressed by combining analytical models of actuator kinematics, actuator force, drive torque, traction and static stability with repeated stair trials and a trial-level failure analysis.

1.1. Research Gap

A review of the stair-climbing wheelchair literature (Section 2) indicates the following gaps:

- Few low-cost stair-climbing wheelchair prototypes integrate IoT monitoring (GPS tracking and cloud-based remote override) with a motorized stair-negotiation mechanism and report quantitative stair-climbing results.
- Limited prototype-level data are available for staircase geometries typical of Egyptian and North African residential buildings.
- The drive-torque, traction and stability margins of low-cost BLDC hub-motor and linear-actuator combinations during stair negotiation have not been systematically quantified.
- Trial-level reporting of failure modes is rare, although it is essential for assistive devices in which reliability is safety-critical.

1.2. Research Objectives

To close these gaps, the work was organised around three objectives:

- Build a low-cost mechatronic stair-climbing wheelchair that an attendant can guide up a typical Egyptian residential staircase, with an embedded NodeMCU ESP8266 layer for remote supervision (GPS location, Wi-Fi override and an obstacle stop for level-ground driving).
- Develop analytical models of actuator kinematics and force, drive torque, power budget, traction and static stability, and check their predictions against laboratory measurements.
- Measure how reliably the prototype climbs with and without a 70 kg load, locate where and explain why ascents fail, and turn these findings into quantified design corrections.

1.3. Contributions

The contributions of this work are as follows:

- The integration of a NodeMCU ESP8266-based IoT layer (Blynk remote override, GPS tracking and infrared obstacle stop for level-ground driving) with a motorized stair-tread wheelchair platform built from commercially available components at a prototype component cost of USD 350–450. The contribution lies in this integration and its evaluation, not in a new stair-climbing mechanism.
- A consistent analytical framework (actuator kinematics, actuator free-body force, drive-torque demand, power budget, traction requirement and static stability margin) that explains why the prototype succeeded in all unloaded trials but failed in three of ten loaded trials.
- A trial-level experimental dataset (n = 10 per load condition) with exact binomial confidence intervals and failure-mode characterisation (Table 4).
- Specific, quantified design corrections (drive-torque margin, tread friction, stabilisation and fail-safe braking) for the next prototype iteration.

2. LITERATURE REVIEW

2.1. Classification of Stair-Climbing Mechanisms

Stair-climbing wheelchair mechanisms are commonly classified into wheel-cluster, legged, tracked and balancing types [3]. Lawn and Ishimatsu [6] modelled a wheel-cluster mechanism with high single-step capability and validated it on a scale prototype. Morales et al. [7] developed a wheelchair with two mechanically decoupled axle mechanisms whose coordinated actuation keeps the seat level on stairs, achieving high versatility at the cost of mechanical and control complexity. Cho et al. [8] combined a tri-spoke wheel cluster with a supporting leg and derived design equations that account for wheel–stair collisions; their 120 kg prototype climbed and descended stairs with 180 mm risers and 300 mm treads at about ten steps per minute. Quaglia et al. [10] proposed Wheelchair.q, whose self-adaptive locomotion units change passively from rolling on wheels to walking on rotating legs when a step is encountered. Akamisaka and Nagao [11] proposed a transformable quadruped wheelchair that walks on its legs during stair ascent and descent, with the stair-climbing gait trained by reinforcement learning in simulation.

Tracked (crawler) systems distribute the load over several stair nosings and tolerate variations in step geometry, but they are heavy and often require backward ascent [3,12]. Sharma et al. [12] presented a semi-autonomous tracked wheelchair with pose estimation and seat-posture adjustment. Pappalettera et al. [13] proposed a tracked stair-climbing platform with bogie-type suspensions, analysed it by multibody simulation and suggested it as a wheelchair base; the same group surveyed wheeled, tracked, legged and hybrid stair-climbing vehicles in [15]. Balancing platforms such as the iBOT climb stairs dynamically but require redundant sensing and control and have been costly [14]. Clinical and biomechanical evaluations of stair-climbing wheelchairs show that user stability and perceived safety on stairs are the principal acceptance factors [16,23]. Related work on assistive mobility for people with spinal cord injury or lower-limb weakness, such as saddle-assistive devices with mechanical orthoses and body-weight-supported wheeled walkers, likewise emphasises load-path design and user safety [24–27].

2.2. IoT Integration in Assistive Mobility Devices

The availability of inexpensive Wi-Fi microcontrollers and cloud platforms has accelerated IoT integration in assistive devices [17]. Simpson [18] and Leaman and La [19] identified obstacle avoidance, navigation assistance and remote monitoring as recurring functions of smart wheelchairs. Recent IoT wheelchair prototypes combine microcontroller-based control with wireless health and location monitoring [20] or smartphone-based telemonitoring of seat-positioning functions [21], and remote-monitoring and digital-twin architectures developed for other mechatronic systems provide transferable patterns for data acquisition and remote control [22].

Obstacle detection in powered wheelchairs has been implemented with ultrasonic, infrared and LiDAR sensing [19]. Infrared proximity sensors such as the E18-D80NK provide a low-cost digital output with an adjustable range of up to about 80 cm and are directly compatible with microcontroller inputs, but their performance depends on target reflectivity and ambient infrared light. Human-centred frameworks for evaluating safety in intelligent automated vehicles [28] emphasise that such sensing functions must be judged by the safety outcomes they deliver, which motivates the explicit treatment of emergency stop, rollback and sensor effectiveness in the present study.

2.3. Accessibility Context in Egypt

Persons with disabilities in Greater Cairo report physical barriers in public places, including stairs, discontinuous pavements and inaccessible entrances [5], and access to assistive products in low- and middle-income countries is constrained by cost, supply and maintenance capacity [2,4]. These conditions motivate wheelchairs that can negotiate existing staircases rather than depend on environmental modification.

Table 1 compares the main stair-climbing mechanism categories with the proposed SCW.

Table 1: Comparative analysis of stair-climbing wheelchair mechanism categories and performance characteristics of the proposed SCW relative to prior work.

Mechanism Type	Stair Autonomy	Terrain Versatility	Load Capacity	Commercial Status
Tracked crawler	Full	High	High	Limited
Leg-type	Full	Very High	Medium	Rare
iBot balancing	Full	High	Medium	Relaunched; limited availability
Hybrid wheel-cluster	Partial (assisted)	High	High	Moderate
Proposed SCW (this work)	Attendant-supervised, semi-automatic (motorized tread)	Moderate (regular stairs; one geometry tested)	Design payload 100 kg (130 kg total); tested 70 kg	Laboratory prototype

3. METHODS

3.1. System Architecture Overview

The prototype was built around two design choices: a single low-cost Wi-Fi microcontroller (NodeMCU ESP8266) that handles both real-time control and cloud communication, and commercial off-the-shelf drive and actuation modules that can be replaced individually. Functionally, the system is described in three layers (Figure 1). The mechanical layer comprises the steel frame, the two rear stair-tread assemblies with their linear actuators, and the hub-motor drive wheels. The electrical layer comprises the $LiFePO_4$ battery, the main contactor, fuse and hard-wired emergency stop, the two commercial BLDC motor controllers, the 24/12 V DC–DC converter and the relay modules. The sensing and IoT layer comprises the joystick, the E18-D80NK infrared obstacle sensor (active during level-ground driving only), the NEO-6M GPS module and the Blynk link to the caregiver's smartphone. The NodeMCU reads the sensors, runs the 20 Hz control loop, sends the throttle, direction and enable signals to the motor controllers (through the L293D logic buffer and the relays), switches the actuator relays and exchanges data with the Blynk cloud. No second microcontroller is used.

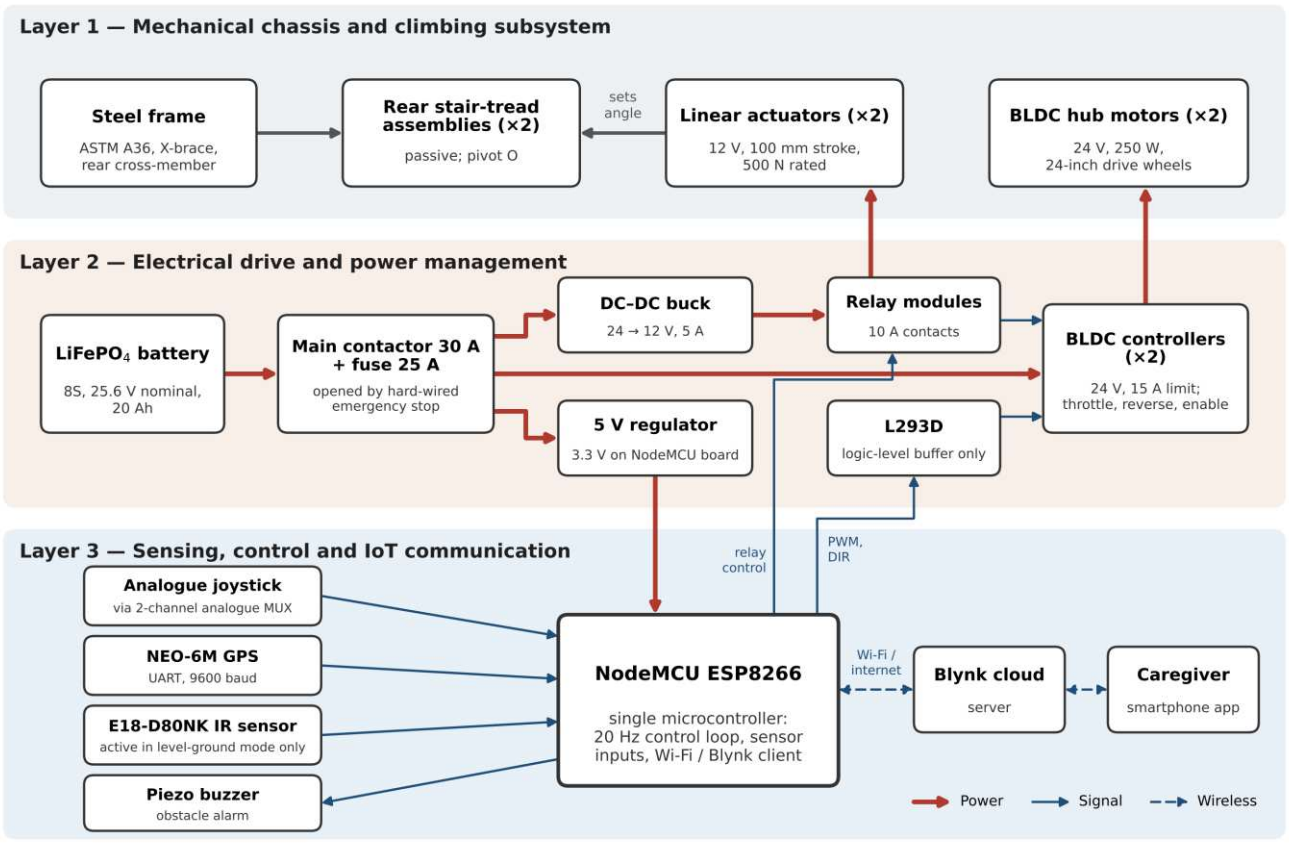


Figure 1: SCW system architecture block diagram. A single NodeMCU ESP8266 performs both control and IoT communication; the L293D only buffers the throttle and direction signals to the two commercial 24 V / 15 A BLDC controllers, which drive the hub motors; the hard-wired emergency stop opens the main contactor; and the single E18-D80NK infrared sensor is active during level-ground driving only.

3.2. Mechanical Design

3.2.1. Frame and Structural Design

The wheelchair frame was fabricated from ASTM A36 structural steel using MIG welding, providing a balance between structural rigidity, fabrication simplicity and low cost. The frame follows the conventional folding X-brace topology, with reinforced joints at the stair-climbing attachment points to accommodate the additional loading during stair ascent and descent. A rigid cross-member was added at the rear of the frame to serve as the mounting interface for the stair-tread mechanism and the linear actuators. The frame mass was 8.2 kg, the wheelchair assembly excluding the battery weighed approximately 22 kg, and the complete prototype as tested (including battery and stair-climbing mechanism) weighed approximately 30 kg (Table 3).

3.2.2. Stair-Tread Climbing Mechanism

The stair-climbing subsystem employs a motorized stair-tread principle in which a pair of electric linear actuators sets the angle of a rear-mounted tread (track) assembly to conform to the staircase pitch. The motorized stair-tread approach was selected from the mechanism categories in Table 1 for its low cost and its suitability for attendant-supervised operation. Figure 2 shows the SolidWorks assembly and Figure 3 the kinematic schematic and free-body diagram of the mechanism.

Mechanism description. Each of the two rear tread assemblies (Figure 2) is connected to the rear cross-member through a pivot O. A linear actuator connects a frame anchor A to a bracket B on the tread assembly, so that actuator extension rotates the assembly about O and sets the tread angle relative to the seat frame. The treads

are passively guided (not driven); propulsion is provided by the rear hub motors. Ascent is in the forward direction with attendant supervision. The tread angle is set in open loop by the actuators, which stop at their internal end-of-stroke limit switches; no angle sensor is fitted to the present prototype.

Climbing sequence. (i) Approach: the attendant aligns the wheelchair perpendicular to the first riser at low speed; (ii) deployment: the actuators extend to set the tread angle to the stair pitch ($\theta_{stair} \approx 32°$), bringing the tread contact line onto the first stair nosings; (iii) ascent: the hub motors drive at reduced speed while the tread assembly advances along the nosings; (iv) terminal step: when the rear support reaches the top landing, the actuators retract so that the drive wheels regain contact with the landing; (v) exit: the chair is driven clear of the stair edge. Descent follows the reverse sequence. An attendant stands behind the chair throughout and holds the push handles during stages (ii)–(iv).

Two commercially available 12 V DC linear actuators (100 mm stroke, 500 N rated dynamic load, 2 A rated current, ≈10 mm/s no-load speed, self-locking lead screw) are used. The mechanism was dimensioned for typical Egyptian residential staircases with riser height H_r = 150–175 mm and tread depth D_t = 250–300 mm, i.e. a pitch angle $\theta_{stair} = \arctan(H_r/D_t) \approx 27°–35°$. Only the 175/275 mm geometry ($\theta_{stair} = 32.5°$) was tested experimentally (Section 5); the required actuator extension is derived in Section 4.1.

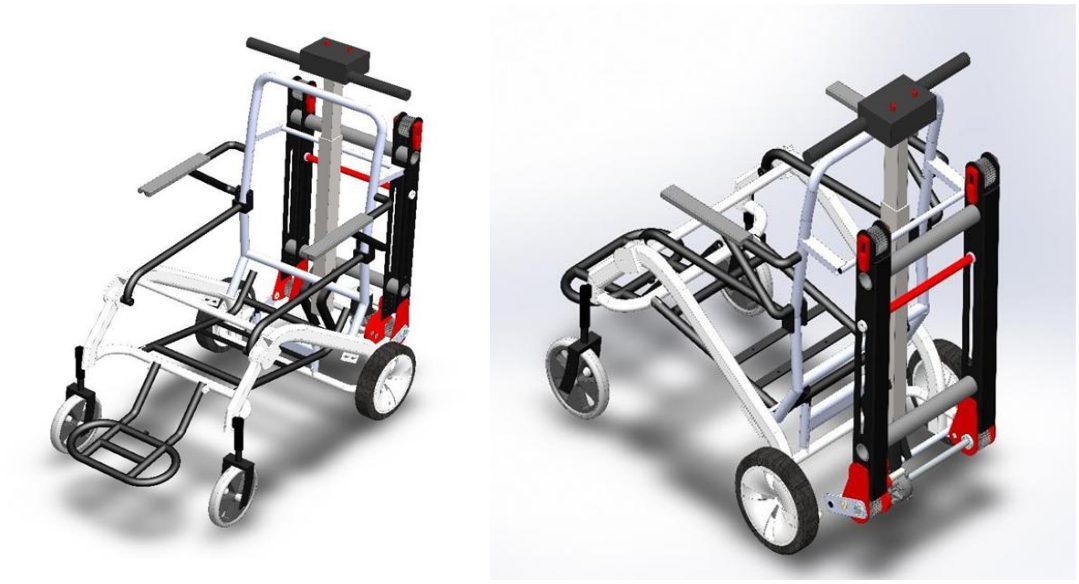


Figure 2: SolidWorks Assembly Design.

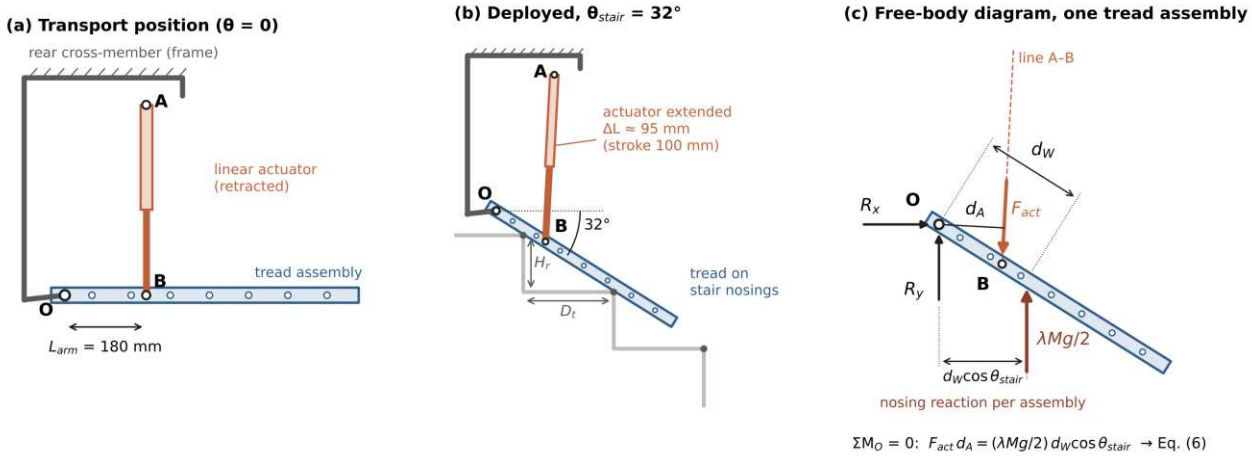


Figure 3: Motorized Stair-Tread Mechanism — Kinematic Schematic and Free-Body Diagram.

(a) Transport position ($\vartheta = 0$), showing pivot O, frame anchor A, tread bracket B and the effective arm L_{arm} = 180 mm; (b) deployed position on the design staircase (ϑ_{stair} = 32°, H_r = 175 mm, D_t = 280 mm), with the required actuator extension ΔL ≈ 95 mm (Eq. 2) within

the 100 mm stroke; (c) free-body diagram of one tread assembly showing the actuator force F_{act} along A–B at perpendicular distance d_A, the nosing reaction $\lambda Mg/2$ acting at d_W along the tread (moment arm $d_W \cdot \cos \vartheta_{stair}$) and the pivot reactions R_x, R_y (Section 4.3). Schematic, not to scale.

3.2.3. Drive Wheels and Caster System

Propulsion is provided by two 24 V brushless DC hub motors (250 W rated power; 45 N·m rated continuous torque; peak torque 85 N·m for up to 30 s; manufacturer specifications) integrated into 24-inch rear drive wheels. Hub motors were selected because they require no external transmission and little maintenance, which is important where specialised technicians are scarce. The front caster wheels (6-inch diameter, polyurethane tyre) provide passive steering support. The differential drive enables turning on the spot by driving the two rear motors in opposite directions under joystick control (Section 4.6).

3.3. Electrical System

3.3.1. Control Architecture

The NodeMCU ESP8266 module is the central processing unit of the SCW. The ESP8266 SoC integrates a 32-bit Tensilica L106 processor operating at up to 160 MHz, 802.11 b/g/n Wi-Fi and the GPIO pins accessible through the NodeMCU board. Because the ESP8266 provides a single 10-bit ADC channel (0–3.3 V on the NodeMCU board), the two joystick potentiometers (X- and Y-axis) are read through an external 2-channel analogue multiplexer. The control loop executes at 20 Hz, and joystick deflections are mapped to differential motor speed commands with a ±50 ADC-count dead zone (Section 4.6).

3.3.2. Motor Driver and Relay Management

Each hub motor is driven by a commercial 24 V sensored BLDC controller with a 15 A current limit (typical for 250 W hub motors) that performs electronic commutation internally. The NodeMCU sets motor speed through a PWM signal applied directly to the controller's 0–5 V throttle input, and sets direction through the controller's reverse input. The L293D is used only as a logic-level buffer (3.3 V to 5 V) for these throttle and direction signals and carries no motor current, consistent with its 600 mA per-channel rating. The relay modules (10 A contacts) switch (i) the controllers' enable lines and (ii) the polarity of the 12 V actuator supply for extension and retraction; they do not carry hub-motor current. The hub-motor current passes through a 30 A main contactor and a 25 A fuse, both rated above the battery current at rated motor power (21.8 A; Table 2) and above the measured battery current during loaded climbing (≈15 A). Both ratings, however, lie below the worst-case battery current of ≈32.3 A that results when both controllers operate at their 15 A current limits (Section 4.5). No fuse operation occurred in any trial; in the next iteration the main fuse will be replaced by a 40 A time-delay type and the contactor up-rated to 40 A, so that this worst case is covered without nuisance tripping. The emergency-stop push button opens the main contactor coil circuit, removing power from both motor controllers and the actuators independently of the software, following the stop-category principles of IEC 60204-1 [29].

Emergency stop during stair climbing. Removing power on the staircase does not by itself hold the wheelchair: the lead-screw actuators are self-locking and maintain the tread angle, but unpowered hub motors without electromagnetic brakes can be back-driven, creating a risk of rollback. In the present prototype this risk is mitigated only by the attendant, who holds the push handles throughout the climb. Power-off-engaged electromagnetic brakes will therefore be fitted to the drive motors in the next iteration, and their ability to hold the loaded chair on the 32.5° pitch after an emergency stop will be verified (Section 10).

3.3.3. Power System

The primary power source is a 24 V (8 S, 25.6 V nominal) LiFePO4 battery with a nominal capacity of 20 Ah (≈8 kg). $LiFePO_4$ chemistry was selected for its thermal stability and cycle life relative to other lithium-ion chemistries [30,31]. Charging uses a CC–CV charger with cut-off at 29.2 V. The constant-current charging time from 20% state of charge at I_{charge} = 5 A is $t_{charge} \approx \Delta SOC \cdot C_{Ah}/(I_{charge} \cdot \eta_{charge}) = 0.8 \times 20/(5 \times 0.95) \approx 3.4$ h, followed by a short constant-voltage phase (≈4 h in total). The 12 V actuators are supplied through a 24 V to 12 V DC-DC buck converter (5 A rating, $\eta_{DC} \approx 0.90$).

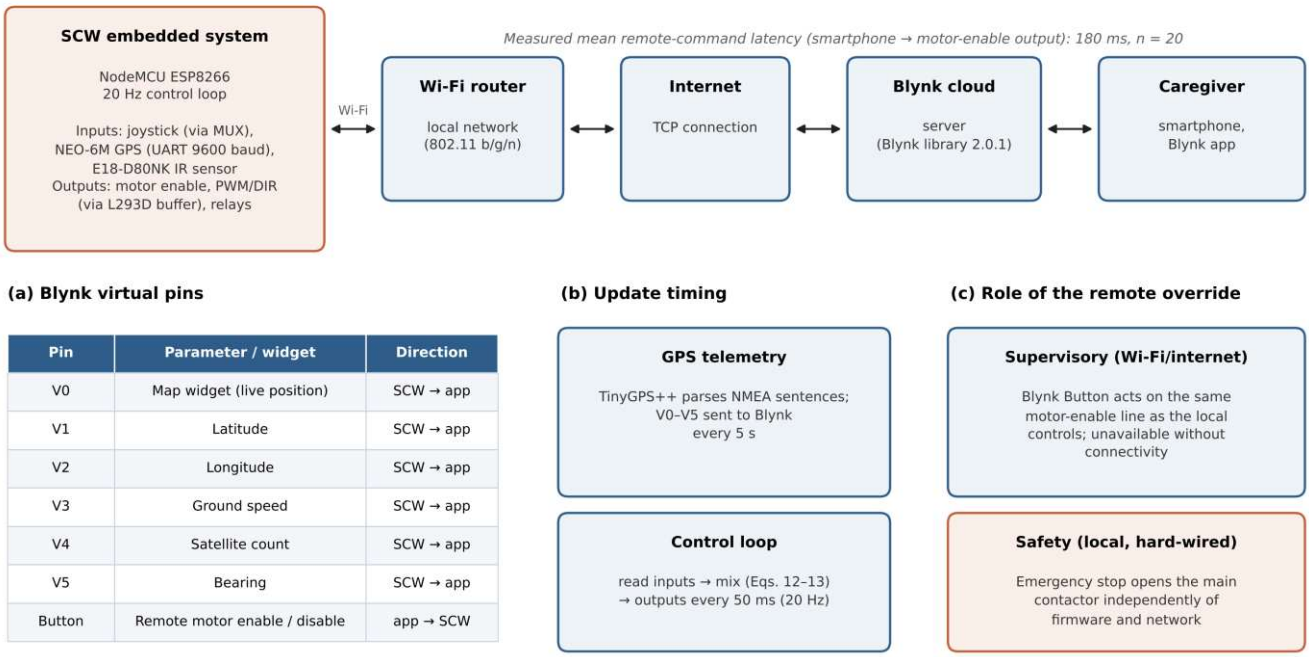
3.3.4. Sensing Subsystem

Obstacle detection is provided by an E18-D80NK infrared reflective proximity sensor mounted at the front of the frame 30 cm above the floor. The sensor provides a digital NPN output: logic LOW when no obstacle is detected within its adjustable range (3–80 cm) and logic HIGH upon detection. Upon a HIGH event, the NodeMCU clears the motor-enable output and activates a piezoelectric buzzer. The infrared obstacle stop is inhibited during stair negotiation to avoid false triggers from the risers, so the present prototype has no stair-edge or drop-off detection while climbing; downward-facing distance sensors and an IMU-based climbing interlock are planned for the next iteration (Sections 6.4 and 10).

GPS localisation is provided by a u-blox NEO-6M module (datasheet horizontal accuracy 2.5 m CEP [32]) communicating via software serial UART at 9600 baud. The TinyGPS++ library (version 2.0.1) parses the NMEA sentences, extracting latitude, longitude, ground speed, satellite count and bearing, which are transmitted to the Blynk platform via Wi-Fi at 5 s intervals for caregiver location monitoring.

3.4. IoT Communication and Remote Control

The Blynk IoT platform provides the cloud communication backbone for the SCW. The Blynk firmware library (version 2.0.1), executing on the NodeMCU, maintains a persistent TCP connection to the Blynk cloud server over Wi-Fi. Virtual pin V0 is mapped to the Blynk Map widget for real-time GPS display, and virtual pins V1–V5 transmit latitude, longitude, ground speed, satellite count and bearing, respectively. A Blynk Button widget provides a remote motor enable/disable override that acts on the same enable line as the local controls; it does not bypass the hard-wired emergency stop and, because it depends on internet connectivity, it is a supervisory rather than a safety function. Location-aware caregiver alerts during stair negotiation are not implemented in the present prototype and are planned future work. Figure 4 illustrates the IoT communication workflow.



Pin	Parameter / widget	Direction
V0	Map widget (live position)	SCW → app
V1	Latitude	SCW → app
V2	Longitude	SCW → app
V3	Ground speed	SCW → app
V4	Satellite count	SCW → app
V5	Bearing	SCW → app
Button	Remote motor enable / disable	app → SCW

Figure 4: IoT Communication Architecture and Blynk Platform Integration

Communication chain: SCW embedded system (NodeMCU ESP8266) ↔ Wi-Fi router ↔ Internet ↔ Blynk cloud server ↔ caregiver smartphone app. (a) Blynk virtual-pin assignments (V0 map widget; V1–V5 latitude, longitude, ground speed, satellite count and bearing; Button widget for remote motor enable/disable); (b) update timing (GPS telemetry every 5 s; control loop every 50 ms, 20 Hz); (c) distinction between the supervisory remote override, which depends on connectivity, and the local hard-wired emergency stop.

4. MATHEMATICAL MODELLING

4.1. Staircase Geometry and Actuator Kinematics

Let the staircase be characterized by riser height H_r and tread depth D_t. The staircase inclination angle is:

$$\theta_{\text{stair}} = arctan\,(H_r/D_t) \qquad (1)$$

For the design staircase, taken at the maximum riser height of the typical Egyptian residential range with a mid-range tread depth (H_r = 175 mm, D_t= 280 mm), θ_{stair} ≈ 32°; the laboratory test staircase (H_r = 175 mm, D_t = 275 mm) has θ_{stair} = 32.5°, and both geometries are used below. The required linear actuator extension ΔL to lower the stair-tread platform from its neutral horizontal position to the staircase approach angle is:

$$\Delta L = L_{arm} \times sin(\theta_{\text{stair}}) \qquad (2)$$

where L_{arm} is the effective moment arm, i.e. the perpendicular distance from pivot O to the actuator line of action in the transport position. Equation (2) is a first-order approximation that assumes the actuator remains approximately perpendicular to the arm. For the prototype, the effective arm is L_{arm} = 180 mm; this single value is used throughout the paper and in Figure 3. Equation (2) gives ΔL = 180 × sin 32.0° ≈ 95 mm for the design staircase and 180 × sin 32.5° ≈ 97 mm for the test staircase. Both predictions lie within the 100 mm actuator stroke, although the margin is small (≈3–5 mm). At the steep end of the dimensioned range (H_r = 175 mm, D_t = 250 mm, θ_{stair} ≈ 35°), however, Eq. (2) gives ΔL ≈ 103 mm, which exceeds the stroke; with L_{arm} = 180 mm the 100 mm stroke covers pitch angles up to arcsin(100/180) ≈ 33.7° only. The measured extension at full deployment was 92 ± 3 mm (mean ± SD, n = 10), 3–5% below the first-order prediction; the difference is attributed to mounting clearance and to the tread contacting the nosings before reaching the full pitch angle.

4.2. Drive Motor Torque Requirements

The torque requirement for each rear hub motor during stair ascent is estimated from the quasi-static equilibrium of the wheelchair system. For total system mass M (wheelchair + occupant) on a staircase of inclination θ, the propulsive force F_p required at the drive wheel circumference is:

$$F_p = M \times g \times (\sin\theta + \mu_r \times \cos\theta) \qquad (3)$$

where μ_r is the rolling resistance coefficient (≈ 0.02) and g = 9.81 m/s². For the design case, substituting M = 130 kg (≈30 kg prototype mass + 100 kg design payload; Tables 1 and 3) and $\theta = 32°$:

$$F_p = 130 \times 9.81 \times (\sin 32° + 0.02 \times \cos 32°) \approx 697\ N \quad (4)$$

For each of the two drive wheels (radius r_w = 0.305 m corresponding to 24-inch wheels):

$$T_{motor} = F_p \times r_w / 2 = 697 \times 0.305 / 2 \approx 106\ N \cdot m\ per\ motor \quad (5)$$

Equations (3)–(5) give the quasi-static drive-torque demand under the conservative assumption that the drive wheels carry the full gravity component along the stair pitch line. For the design case (M = 130 kg, θ = 32°) the demand is ≈106 N·m per motor. For the loaded test case (M = m_{SCW} + 70 kg ≈ 100 kg, θ = 32.5°) it is ≈83 N·m, and for the unloaded test case (M ≈ 30 kg) it is ≈25 N·m.

These demands must be compared with two distinct limits of the motor: the continuous (rated, thermally sustainable) torque of ≈45 N·m, and the short-duration peak torque of 85 N·m set by the controller current limit, permissible for up to 30 s according to the manufacturer's specification. The design-case demand (≈106 N·m) exceeds even this peak rating by ≈25%, so the present drive cannot carry the full 100 kg design payload on the design staircase; the loaded tests were limited to 70 kg. Reducing the commanded speed does not increase the available torque, which is limited by the controller current and the motor thermal capacity. The peak torque during loaded ascent, estimated from the measured motor current as T ≈ K_t·I (current measured with an ACS712 Hall-effect current sensor at 10 Hz sampling rate), was 83 N·m per motor, within 3% of the quasi-static prediction for the tested mass. Because this estimate relies on an assumed torque constant K_t rather than an independent torque measurement, the agreement indicates consistency with Eq. (5) rather than independent validation. Operation this close to the peak-torque limit leaves little margin for step-to-step variations and is identified in Section 6.1 as a contributing factor to the loaded failures; motor temperature was not measured, so thermal safety under repeated climbs remains to be verified.

4.3. Actuator Force and Free-Body Analysis

Figure 3c shows the free-body diagram of one tread assembly during climbing. The assembly is loaded by (i) the share λ of the total weight Mg transmitted through the tread contact with the stair nosings, acting at lever arm d_W about pivot O, (ii) the actuator force F_{act} acting along A–B at perpendicular distance d_A from O, and (iii) the pivot reaction components (R_x, R_y). Assuming that the two actuators share the load equally, moment equilibrium about O gives

$$F_{act} = \lambda \cdot M \cdot g \cdot dW \cdot \cos\theta_{stair} / (2 \cdot dA) \qquad (6)$$

With the CAD dimensions d_W =250 mm (estimated) and d_A = 180 mm and assuming equal load sharing between the two actuators and the load share λ = 0.5, Eq. (6) gives F_{act} ≈ 287 N for the tested mass M ≈ 100 kg (θ_{stair} = 32.5°), i.e. a safety factor SF = 500 N/F_{act} ≈ 1.74 against the rated dynamic load. For the 130 kg design mass (θ_{stair} = 32°) the actuator force rises to ≈ 376 N and SF ≈ 1.33. A safety factor of at least 1.5 requires $\lambda \cdot dW \cdot \cos\theta_{stair}/dA \leq 0.68$ for the tested mass (≤ 0.52 for the 130 kg design mass), which provides a direct geometric design check for the mechanism. The present geometry gives λ·d_W·cos θ_{stair}/d_A ≈ 0.59, which satisfies the check for the tested mass but not for the 130 kg design mass; increasing d_A to at least 203 mm, or using actuators rated at least 565 N, would restore SF ≥ 1.5 at the design mass.

4.4. Traction and Static Stability on the Staircase

Traction. When the tread assembly rests on the stair nosings, propulsion along the pitch line relies on friction between the tread surface and the nosings. Neglecting rolling resistance, the minimum friction coefficient required to hold or advance the wheelchair on the pitch line is

$$\mu_{req} = \tan \theta_{stair} \qquad (7)$$

which equals 0.64 for the test staircase (θ_{stair} = 32.5°). The static friction coefficient of smooth rubber on concrete is $\mu_s \approx 0.65$ (typical literature value for this material pair [33]; not measured on the test nosings), leaving a margin of only ≈2% over μ_{req}. Although μ_{req} is independent of mass, any reduction of the normal force at an individual nosing, which is most pronounced at the terminal step where only one nosing remains in contact, makes slip more likely as the tangential force increases with load.

Static stability. Backward tip-over about the rear-most support contact occurs when the vertical line through the combined centre of gravity G passes behind that contact. With x_G the distance of G ahead of the rear contact measured parallel to the support line and z_G its height normal to that line, the static stability margin angle is

$$\beta = \arctan(x_G/z_G) - \theta_{eff} \qquad (8)$$

where θ_{eff} is the inclination of the support line (θ_{stair} on the flight, changing towards 0 at the terminal-step transition); $\beta > 0$ indicates static stability. With the CoG positions estimated from the preliminary CAD model (unloaded: $x_G \approx 200$ mm, $z_G \approx 450$ mm; loaded: $x_G \approx 220$ mm, $z_G \approx 470$ mm), $\arctan(x_G/z_G) \approx 24.0°$ unloaded and 25.1° loaded, so that Eq. (8) gives $\beta \approx -8.5°$ (unloaded) and $\beta \approx -7.4°$ (loaded) on the 32.5° flight. These negative margins indicate that, according to these estimates, the chair is not statically self-stable on the flight and depends on the attendant, who held the push handles during every ascent (Section 3.2.2); once the support line becomes level at the top landing ($\theta_{eff} \rightarrow 0$), β rises to ≈24–25°. Because the seat load moves G forward as well as upward, the estimates do not show a lower margin under load, so static stability does not by itself explain why only loaded ascents failed. The CoG coordinates were not measured, and these margins are therefore provisional. ISO 7176-1 and ISO 7176-28 specify the static-stability and stair-climbing-device test methods against which these margins should ultimately be verified [34,35].

4.5. Power Budget and Battery Runtime

Table 2 lists the voltage, current, power, duty cycle and supply path of every load. The drive motors (2 × 250 W rated) are supplied from the battery through their controllers. The 12 V actuators (2 × 12 V × 2 A = 48 W) are supplied through the 24 V to 12 V DC–DC converter, so their battery-side power is $48/\eta_{DC} \approx 53$ W for $\eta_{DC} \approx 0.90$. The control electronics draw ≈5 W. The battery power and current at rated motor power are therefore

$$P_{total} = 500 + 53 + 5 = 558\ W \qquad (9)$$

$$I_{peak} = P_{total} / V_{batt} = 558 / 25.6 \approx 21.8\ A \qquad (10)$$

Equations (9) and (10) are based on the rated motor power. Fuse and contactor sizing must also cover the worst case in which both controllers operate at their 15 A current limits, as they may during loaded climbing close to the peak-torque limit (Section 4.2): $P_{max} \approx 2 \times 15\ A \times 25.6\ V + 53\ W + 5\ W \approx 826$ W, i.e. $I_{max} \approx 32.3$ A. The measured battery current during loaded climbing (≈15 A, see below) remained well below both values.

The usable energy is $E = V_{batt} \cdot C_{Ah} \cdot DoD = 25.6 \times 20 \times 0.9 \approx 461$ Wh. For a deliberately conservative duty cycle (level driving at 50% motor load for 75% of the operating time and stair climbing at full load for 25%), the average power is $P_{avg} = 0.75 \times (250 + 5) + 0.25 \times 558 \approx 331$ W, corresponding to an average battery current of ≈12.9 A and a runtime of

$$t_{eff} = E / P_{avg} \approx 461 / 331 \approx 1.4\ h \qquad (11)$$

The measured battery current was approximately 5 A during level driving and 15 A during loaded stair climbing. For the same duty cycle this gives an average current of 0.75 × 5 + 0.25 × 15 = 7.5 A and a runtime of 18 Ah / 7.5

A ≈ 2.4 h, where 18 Ah is the usable capacity (20 Ah × 0.9). Equation (11), which assumes rated power throughout, therefore gives a conservative lower bound (≈1.4 h). Because a 25% share of stair climbing is far above typical daily use, the practical runtime depends strongly on how often stairs are climbed.

Table 2: Power budget of the SCW prototype. Rated values are shown; measured currents are reported in Section 4.5 together with the worst-case controller-limited current (≈32.3 A).

Load	Voltage (V)	Current (A)	Power (W)	Duty cycle	Supply path
BLDC hub motors (×2)	24 (25.6 nom.)	2 × 9.8 rated; 2 × 15 limit	500 rated	Driving and climbing	Battery → contactor/fuse → BLDC controllers
Linear actuators (×2)	12	2 × 2.0 rated	48 (≈53 battery side)	Tread deployment/retraction only	Battery → 24/12 V DC–DC converter (η ≈ 0.90) → relays
NodeMCU, GPS, IR sensor, relay coils, buzzer	3.3–5	≈0.2 at 24 V	≈5	Continuous	Battery → 5 V regulator (→ 3.3 V on board)
Total (rated)	25.6	≈21.8 (Eq. 10)	≈558 (Eq. 9)	—	—

4.6. Joystick ADC Mapping and Differential Drive Control

The analog joystick provides dual-axis potentiometer outputs (X, Y), each varying from 0 to 1023 ADC counts across full deflection. The neutral position corresponds to approximately 512 counts. Differential motor speed commands are computed as:

$$V_{right} = k \times [(Y - 512) + (X - 512)] \quad (12)$$

$$V_{left} = k \times [(Y - 512) - (X - 512)] \quad (13)$$

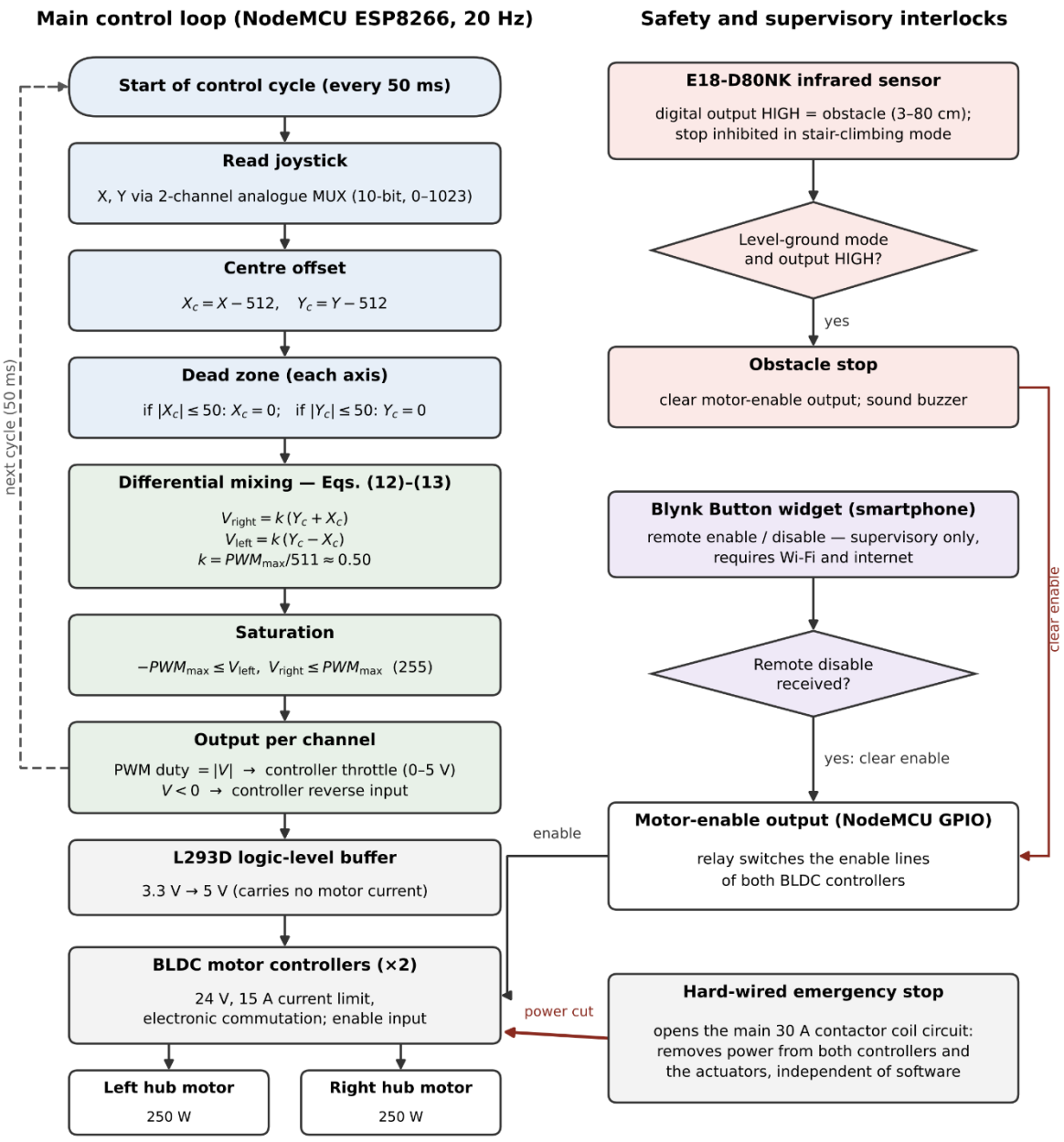


Figure 5: Joystick ADC Mapping and Differential Drive Control Flowchart. The L293D only buffers the throttle and direction signals to the BLDC controllers; the obstacle stop and the Blynk disable act on the motor-enable output, and the hard-wired emergency stop removes power independently of the firmware.

where k = PWM_{max}/511 is the scaling constant (k ≈ 0.50 for 8-bit PWM with PWM_{max} = 255), and each command is saturated to ±PWM_{max}; negative commands set the controller's reverse input. (Y − 512) is the forward/backward deflection and (X − 512) the turning deflection. Because the turning term enters Eqs. (12) and (13) with opposite signs, a pure X deflection drives the two wheels in opposite directions (turning on the spot), and a combined deflection produces a differential speed and a curved path. Equations (12) and (13) correspond to the implemented firmware. A dead zone of ±50 ADC counts is applied to both axes to suppress motor activation from joystick noise and potentiometer drift. Figure 5 illustrates the joystick-to-motor control flow. The intended turning behavior was verified qualitatively during the level-ground tests (Section 5.2).

5. EXPERIMENTAL SETUP AND PRELIMINARY PROTOTYPE EVALUATION

5.1. Prototype Fabrication

The SCW prototype was fabricated in the Mechatronics Engineering Laboratory, Faculty of Engineering, Heliopolis University, where the original graduation project was conducted. Structural components were cut, drilled and welded from ASTM A36 steel bar stock. The assembly was completed in three stages: (i) frame fabrication and wheel-motor integration; (ii) stair-tread mechanism attachment and actuator installation; and (iii) electrical wiring, PCB installation and sensor mounting. The custom PCB was designed in KiCad EDA (version 6.0) and manufactured by a commercial PCB prototyping service. The mechanical assembly was modelled in SolidWorks (2021), and the firmware was written and compiled in the Arduino IDE (version 1.8.19) with the ESP8266 Arduino core (version 3.0.2). Figure 6 shows the fabricated prototype, and Table 3 consolidates the specifications of the prototype as tested.

*Table 3: Consolidated specifications of the SCW prototype as tested (values marked * are manufacturer ratings; mass, dimensions and speeds were measured on the prototype).*

Component	Specification	Operating Range	Functional Role
NodeMCU ESP8266	80–160 MHz CPU, 802.11 b/g/n Wi-Fi	3.0–3.6 V	Central MCU & IoT gateway
BLDC Hub Motors (×2)	BLDC hub motor, 24 V, 250 W*, 45 N·m rated continuous torque*, 85 N·m peak for 30 s*, external sensored controller	24 V DC (25.6 V nominal)	Rear-wheel propulsion
Linear Actuators (×2)	12 V DC, 100 mm stroke, 500 N rated dynamic load*, 2 A rated*	12 V DC (via 24/12 V converter)	Stair-tread angle adjustment
24 V LiFePO4 Battery	Lithium iron phosphate (8S), 20 Ah nominal, ≈8 kg	20–29.2 V	Primary energy storage
IR Sensor E18-D80NK	Adjustable range 3–80 cm, NPN output	5 V logic	Obstacle detection
GPS Module NEO-6M	NMEA 0183, UART 9600 baud, 2.5 m CEP*	3.3–5 V	Real-time location tracking
L293D Motor Driver	Dual H-bridge, 600 mA/ch*, used as logic buffer only	4.5–36 V	Level shifting of throttle/direction signals
Analog Joystick	Dual-axis potentiometer, 10-bit ADC	3.3 V , 0–1023 counts	Primary user control interface
Relay modules	10 A contacts*	24 V / 5 V coil	Controller enable; actuator polarity
Main contactor + fuse	30 A contactor, 25 A fuse	24 V	Main power path; E-stop disconnection
DC–DC converter	24 V to 12 V buck, 5 A	20–29.2 V in	Actuator supply
Complete prototype	Mass ≈ 30 kg incl. battery (frame 8.2 kg; chair excl. battery 22 kg); L × W × H 1200 × 650 × 950 mm; seat height 500 mm; wheelbase 500 mm; track width 600 mm	—	As tested
Wheels	Rear 24-inch drive (r_w = 0.305 m); front 6-inch PU casters	—	Propulsion; steering support
Payload	Design 100 kg (total design mass ≈130 kg with the 30 kg chair); tested 0 and 70 kg (dead weight)	—	Test condition
Test staircase	5 steps; riser 175 mm; tread 275 mm; pitch 32.5°; concrete; sharp nosing; width 1000 mm	—	Test condition

Operating speed	Level: 1.2 m/s (0 kg), 0.9 m/s (70 kg); climbing: ≈4 s per step	—	Measured



Figure 6: Fabricated SCW Prototype — Front View in the Laboratory (left) and Front and Side Views (right).

5.2. Performance Testing Protocol

Testing was conducted in three functional domains. All tests were laboratory tests without human participants; they constitute a preliminary prototype evaluation and not a clinical validation.

Test environment. All tests were performed indoors in the Mechatronics Engineering Laboratory at ambient laboratory conditions. Level-ground tests were performed on a sealed concrete floor. The test staircase was a reinforced-concrete laboratory staircase with five identical steps (riser 175 mm, tread 275 mm, pitch 32.5°; sharp nosing; concrete surface; width 1000 mm). The simulated occupant load consisted of steel plates totaling 70 kg, strapped to the seat with ratchet straps so that the load center of gravity was centered on the seat; the load position was checked before each trial. The battery was fully charged before each test session, and the battery voltage at the start of each trial was recorded. An attendant stood behind the wheelchair during all stair trials and intervened only to prevent a fall. Each trial was video-recorded at 30 fps for timing and failure analysis. Battery current and voltage were logged with an ACS712 Hall-effect current sensor at 10 Hz. Latencies were measured with a logic analyzer at 1 kHz between the triggering event (sensor output edge or timestamped smartphone command) and the change of the motor-enable output.

- Level-ground mobility: forward, reverse, left-turn and right-turn joystick-controlled driving on the laboratory floor, evaluating steering response, turning on the spot and maximum speed under unloaded and 70 kg loaded conditions (n = 10 per condition).
- Stair-climbing trials: ten ascent trials per load condition (0 kg and 70 kg) on the test staircase; descent trials were not performed. A trial was classified as successful if all five steps were completed without motor stall, tread slip greater than 20 mm, tipping, attendant intervention or displacement of the load. For every trial the steps completed, climbing time, failure mode, attendant intervention and battery energy were recorded; Table 4 lists the outcome, steps completed, failure mode and attendant intervention for each trial.
- Repeated measurements are reported as mean ± standard deviation where the individual values were recorded; for the latency tests only, the mean was logged (Section 6.2). Success rates are reported with exact (Clopper–Pearson) 95% confidence intervals [36], and the loaded and unloaded success rates were compared with a two-sided Fisher's exact test. All statistics were computed in Python 3.10 with SciPy 1.9.0.

- IoT functionality: GPS first-fix acquisition time, Blynk command latency, obstacle-detection response time and remote-override latency were each measured over 20 repeated trials.

5.3. Results Summary

Table 4 lists the trial-level stair-climbing results, and Table 5 summarises all measured performance metrics; Figure 7 compares the measured results with the model predictions, component ratings and design targets.

Table 4: Trial-level stair-climbing results (U = unloaded, L = 70 kg load; ascent of the five-step test staircase). Seven loaded trials were successful and three failed at the terminal-step transition.

Trial	Load (kg)	Outcome	Steps completed	Failure mode	Attendant intervention
U1	0	Success	5/5	—	None
U2	0	Success	5/5	—	None
U3	0	Success	5/5	—	None
U4	0	Success	5/5	—	None
U5	0	Success	5/5	—	None
U6	0	Success	5/5	—	None
U7	0	Success	5/5	—	None
U8	0	Success	5/5	—	None
U9	0	Success	5/5	—	None
U10	0	Success	5/5	—	None
L1	70	Success	5/5	—	None
L2	70	Success	5/5	—	None
L3	70	Fail	4/5	slip	manual push
L4	70	Success	5/5	—	None
L5	70	Success	5/5	—	None
L6	70	Fail	4/5	slip	manual push
L7	70	Success	5/5	—	None
L8	70	Success	5/5	—	None
L9	70	Fail	4/5	slip	manual push
L10	70	Success	5/5	—	None

Table 5: Performance summary of the SCW prototype (laboratory tests).

Performance Metric	Measured Value	Benchmark / Target
Stair success rate (unloaded)	100% (10/10); 95% CI 69–100%	≥95% (design target)
Stair success rate (70 kg load)	70% (7/10); 95% CI 35–93%	≥95% (design target)
Max. level-ground speed (unloaded)	1.2 m/s	—
Max. level-ground speed (70 kg load)	0.9 m/s	—
GPS first-fix time	32 s (open sky)	<60 s (typical)
Blynk command latency	180 ms (n = 20; SD not recorded)	<200 ms (design target)
Obstacle detection response	45 ms (n = 20; SD not recorded)	<200 ms (design target)
Wi-Fi control range	15–30 m	≥15 m (indoor)
GPS positional accuracy	2.5–3.5 m (open sky)	2.5 m CEP (NEO-6M datasheet)
Prototype component cost	USD 350–450	— (component cost only)
Actuator extension at full deployment	92 ± 3 mm	95–97 mm (Eq. 2)
Peak drive torque, loaded ascent	83 N·m (current-based estimate)	83 N·m (Eq. 5, M ≈ 100 kg)

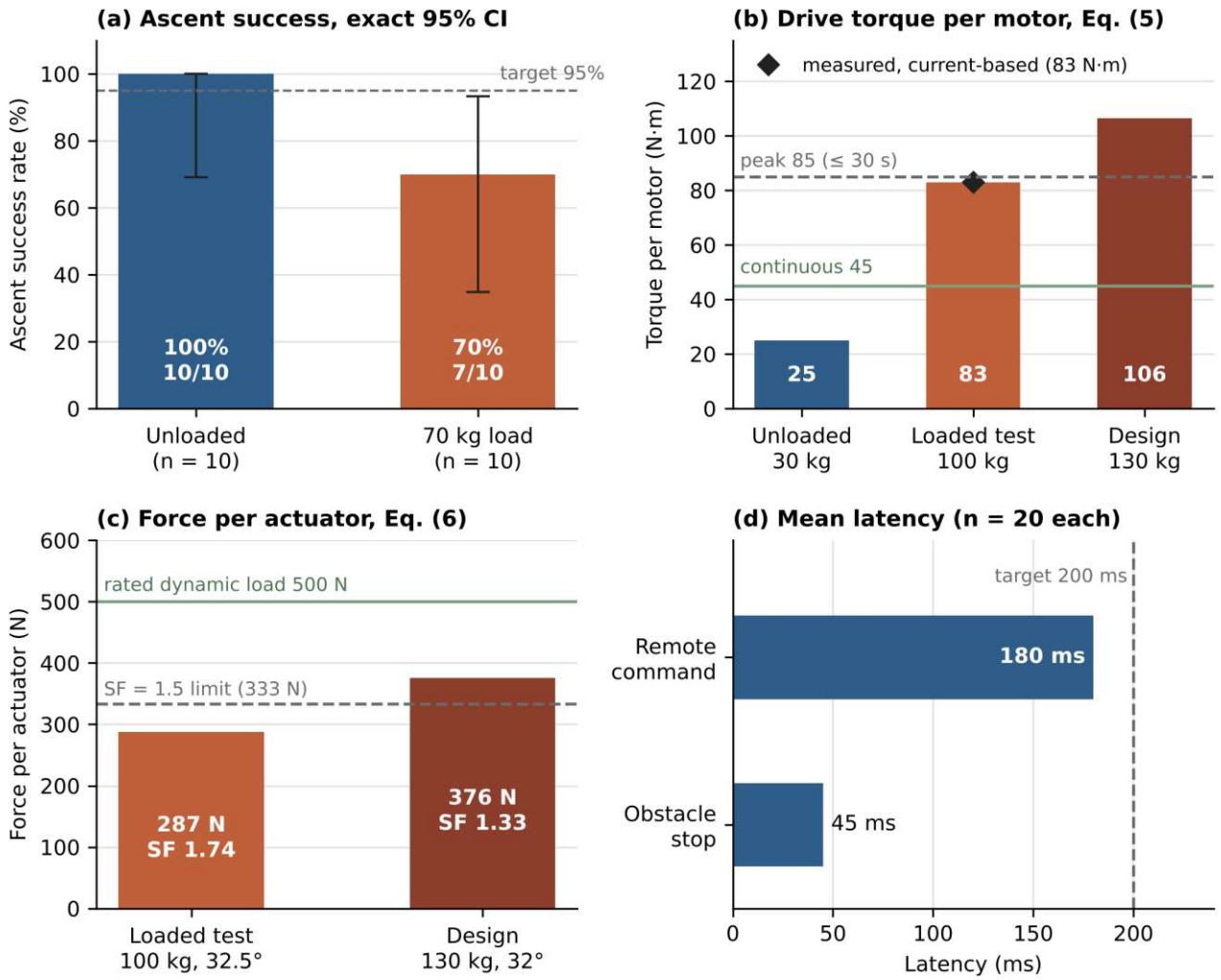


Figure 7: Measured Performance Compared with Model Predictions, Component Ratings and Design Targets

(a) Ascent success rate with exact (Clopper–Pearson) 95% confidence intervals and the 95% design target; (b) quasi-static drive-torque demand per motor (Eq. 5) for the unloaded (30 kg), loaded-test (100 kg) and design (130 kg) cases, with the current-based estimate for the loaded ascent and the 45 N·m continuous and 85 N·m peak ratings; (c) force per actuator (Eq. 6) and safety factor against the 500 N rated dynamic load and the SF = 1.5 limit; (d) mean remote-command and obstacle-stop latencies (n = 20 each) against the 200 ms design target.

6. RESULTS AND DISCUSSION

6.1. Stair-Climbing Performance

All ten unloaded ascents were successful (100%, exact 95% CI 69–100%), whereas seven of ten ascents with the 70 kg load were successful (70%, 95% CI 35–93%). With n = 10 per condition the difference is not statistically significant (Fisher's exact test, p = 0.21), and the wide intervals show that the present data establish feasibility rather than reliability; demonstrating a success rate of at least 95% with 95% confidence would require at least 59 consecutive successful trials (zero-failure binomial criterion).

The models of Section 4 identify two mechanisms that act together at this point and explain why failures occurred only under load, and a third, stability-related limitation that applies with and without load. (i) Drive-torque margin: the loaded ascent requires ≈83 N·m per motor, about 1.8 times the 45 N·m continuous rating and 98% of the 85 N·m short-duration peak rating (consistent with the 83 N·m estimated from the measured current), leaving almost no reserve for the additional effort needed to lift the rear support over the last nosing, whereas the unloaded ascent requires only ≈25 N·m. (ii) Traction: the required friction coefficient on the pitch line (μ_{req} = 0.64) is close to the static friction coefficient assumed for the smooth rubber tread on concrete (μ_s ≈

0.65, literature value [33]), and at the terminal step the normal force is concentrated on a single nosing, so slip becomes likely as the tangential force rises with load; tread slip was the recorded failure mode in all three loaded failures (Table 4). (iii) Static stability: with the preliminary CAD estimates of the centre of gravity, Eq. (8) gives a negative margin on the flight both unloaded ($\beta \approx -8.5°$) and loaded ($\beta \approx -7.4°$), so the chair relied on the attendant throughout; this limitation applies to all trials and must be removed before unsupervised use, but it does not explain the load dependence of the failures. The fact that all failures occurred at the same step, rather than randomly along the flight, indicates a systematic geometric and traction limitation rather than random variability. The measured actuator extension at full deployment (92 ± 3 mm) was within 5% of the first-order kinematic prediction (95–97 mm, Eq. 2), and the current-based peak torque estimate (83 N·m) agreed with the quasi-static prediction for the tested mass (83 N·m, Eq. 5), which shows consistency rather than independent validation (Section 4.2).

Corrective measures derived from this analysis are: a cleated polyurethane tread to raise μ_s above ≈0.8 (a margin of at least 25% over μ_{req}); geared hub motors or an additional reduction stage providing a continuous torque of at least ≈106 N·m per wheel (the quasi-static demand of the 130 kg design case, Eq. 5), preferably ≈130 N·m to retain a 25% margin; an actuator moment arm $d_A \geq 203$ mm or actuators rated ≥ 565 N to restore SF ≥ 1.5 at the design mass; a front stabilisation arm or CoG-shifting seat to obtain a positive margin $\beta \geq 10°$ on the flight and at the terminal step; and a power-off-engaged brake against rollback (Section 10).

6.2. IoT and Remote Monitoring Performance

The mean remote-command latency was 180 ms (n = 20; only the mean was logged, so the standard deviation, range and worst-case value cannot be reported; see Section 8) over the local Wi-Fi network and the Blynk cloud server. Because this path depends on internet connectivity, the remote override is intended as a supervisory function for caregivers and not as a safety function; the safety-relevant stop is provided locally by the hard-wired emergency stop and the obstacle sensor. The GPS module achieved a horizontal accuracy of 2.5–3.5 m under open-sky conditions, consistent with its datasheet specification [32] and sufficient for neighbourhood-level location awareness, but not for indoor or floor-level localisation.

The obstacle-stop latency, measured from the sensor output edge to the clearing of the motor-enable output, was 45 ms (n = 20; only the mean was logged); at 0.9 m/s the chair travels ≈40 mm during this 45 ms interval (0.9 m/s × 0.045 s); the additional deceleration distance of the motors and controllers after the enable output is cleared was not measured and must be added in any stopping-distance assessment. No false-positive detections were recorded in the laboratory, but performance under varying ambient infrared light and with dark or specular obstacles was not tested. During stair negotiation the forward sensor is inhibited and does not detect stair edges or drop-offs; the obstacle function therefore protects level-ground driving only.

6.3. Comparative Analysis with Published Systems

Table 6 compares the SCW qualitatively with representative stair-climbing wheelchairs from the literature. The comparison is limited to features reported in each source; quantitative performance metrics are not directly comparable because the test protocols differ.

Table 6: Qualitative comparison of the proposed SCW with selected stair-climbing wheelchairs from the literature. N/R = not reported.

Study / System	Stair Ascent	Autonomous?	IoT / Remote?	Load (kg)	Cost Level
Lawn & Ishimatsu [6]	Yes (scale)	Yes	No	N/R	Research
Morales et al. [7]	Yes	Yes	No	N/R	Research
Quaglia et al. (Wheelchair.q) [10]	Yes	Passive mode switching	No	N/R	Research
Sharma et al. [12]	Yes (tracked)	Semi-autonomous	No	N/R	Research
iBOT 3000 (Uustal & Minkel) [14]	Yes (balancing)	Partial (user-assisted)	No	N/R	High (commercial)
Proposed SCW (this work)	Yes (motorized)	Attendant-supervised	Yes (Blynk+GPS)	70 tested (100 design)	Low–Med

The wheel-cluster and legged systems [6,7,10] and the tracked system of Sharma et al. [12] offer higher stair-climbing autonomy, as do recent tri-spoke, quadruped and suspended-track designs [8,11,13], and the iBOT has been evaluated in community use [14]; none of these reports IoT remote monitoring. Conversely, IoT wheelchair prototypes [20,21] do not address stairs. The SCW combines a simple, attendant-supervised stair-tread mechanism with low-cost IoT monitoring; its contribution lies in this integration and its quantitative evaluation rather than in a new climbing principle, and its loaded reliability is currently below that expected of a commercial device.

6.4. Safety Considerations and Path to Deployment

The present prototype is not suitable for unsupervised use. Before any user trial, the following safety functions must be implemented and verified: a power-off-engaged electromagnetic brake to prevent rollback after an emergency stop on the stairs; an IMU-based interlock that inhibits climbing when the stability margin β falls below a threshold; stair-edge (drop-off) detection and riser-compatible distance sensing, since the present infrared obstacle stop is inhibited during climbing; and monitoring of motor current and temperature. Verification should follow ISO 7176-1 (static stability) and ISO 7176-28 (stair-climbing devices) [34,35], after which supervised user trials can begin under institutional ethical approval.

7. SUSTAINABILITY-RELATED DESIGN ATTRIBUTES

This section is limited to attributes that can be measured or directly verified on the prototype; broader environmental, economic and social impacts were not measured and are not claimed. A formal life-cycle assessment according to ISO 14040/14044 has not been performed and is planned (Section 10).

Materials and repairability. The frame is made of ASTM A36 structural steel (8.2 kg), a widely available and recyclable material that can be welded and repaired in local workshops. The electrical and electromechanical components (hub motors, controllers, actuators, battery, NodeMCU and sensors) are standard commercial parts connected by plug-in connectors, so each can be replaced individually without special tools. Designing for disassembly and material recovery follows the circular-economy principles discussed in [37].

Energy and battery. The logged battery energy was ≈3 Wh per loaded five-step ascent; as a cross-check, the mean loaded-climbing current (≈15 A at 25.6 V) over the ≈20 s climbing time (≈4 s per step) corresponds to ≈2.1 Wh, the difference presumably reflecting the approach, tread-deployment and retraction phases. The level-ground consumption estimated from the measured current (≈5 A at 25.6 V, i.e. ≈128 W) and the measured speeds (0.9–1.2 m/s) is ≈30–40 Wh/km. The $LiFePO_4$ battery (≈461 Wh usable) contains no cobalt or nickel and offers a long cycle life [30,31]; its end-of-life treatment through established battery-recycling routes is assumed but was not assessed in this study.

Cost. The component cost of the prototype was USD 350–450, excluding labour and certification. This is a prototype component cost and not a retail price; commercial stair-climbing wheelchairs are sold at considerably higher prices, but a like-for-like comparison would require equivalent safety functions and certification.

8. LIMITATIONS

The following limitations of the current work are acknowledged and should be considered in interpreting the reported results:

- Stair climbing was evaluated on a single laboratory staircase (riser 175 mm, tread 275 mm, five steps). Performance on other riser heights, tread depths, nosing profiles, surface materials and irregular staircases has not been established. With L_{arm} = 180 mm, the 100 mm actuator stroke also limits the reachable pitch to ≈33.7°, below the 35° upper end of the dimensioned range.
- Finite-element structural analysis and fatigue-life evaluation of the frame were beyond the scope of the current prototype study and will be included in future iterations.
- The 70% (7/10) success rate under the 70 kg load is insufficient for unsupervised use, and with n = 10 per condition the confidence intervals are wide (Section 6.1). The loaded condition was limited to 70 kg; the 100 kg design payload has not been tested and, according to the models, would exceed the present drive (≈106 N·m demand per motor versus the 85 N·m peak rating) and actuator capacity (SF ≈ 1.33).
- The centre-of-gravity coordinates used in the stability analysis are preliminary CAD estimates; with these values the static margin on the flight is negative, so the chair is not self-stable on the stairs without the attendant. The CoG and the stability margins must be measured on the prototype following ISO 7176-1.
- GPS-based location tracking is limited to outdoor and semi-outdoor environments. Indoor positioning for multi-storey building navigation would require supplementary technologies (BLE beacons, UWB) not implemented in the current prototype.
- No human participants were involved; the results are laboratory prototype results and do not constitute clinical validation. User acceptance, ergonomics and clinical safety have not been assessed.
- No formal safety certification (e.g., ISO 7176 compliance testing) has yet been conducted, which is required prior to clinical or commercial deployment.
- The Wi-Fi-dependent IoT functionality limits the system's remote monitoring capability in locations without Wi-Fi infrastructure. Integration of cellular (4G/LTE) connectivity would address this limitation at modest additional cost.
- Descent performance was not evaluated quantitatively; motor temperature, braking and rollback behaviour after an emergency stop on the stairs were not tested.
- Location-aware caregiver alerts during stair negotiation are not implemented, and the remote override depends on Wi-Fi and internet connectivity.
- For the remote-command and obstacle-stop latencies (n = 20 each) only the mean was logged; the standard deviation, range and worst-case latency, which matter for safety-critical responsiveness, will be recorded in the next test campaign.

9. CONCLUSIONS

This paper has presented the design, mechatronic integration and preliminary laboratory evaluation of a low-cost Smart Climbing Wheelchair (SCW) that combines a motorized stair-tread mechanism, BLDC hub-motor differential drive, joystick control and an ESP8266-based IoT layer for remote monitoring, GPS tracking and obstacle detection for level-ground driving.

The main findings are: (i) the prototype completed all ten unloaded ascents of a 175/275 mm staircase (100%, 95% CI 69–100%) but only seven of ten ascents with a 70 kg load (70%, 95% CI 35–93%); (ii) all loaded failures occurred at the terminal-step transition, with tread slip as the recorded failure mode, and the analytical models indicate that they result from a combination of insufficient drive-torque margin (≈83 N·m demand versus a 45

N·m continuous and 85 N·m peak rating) and marginal tread traction (μ_{req} = 0.64 versus ≈0.65 available); for the 130 kg design case the models predict ≈106 N·m per motor and an actuator safety factor of 1.33, and the preliminary stability estimate shows that the chair is not self-stable on the flight without the attendant; (iii) the kinematic and torque models were consistent with the measured actuator extension and the current-based torque estimate within 5%; and (iv) the IoT layer achieved a mean remote-command latency of 180 ms, an obstacle-stop latency of 45 ms and a GPS accuracy of 2.5–3.5 m at a prototype component cost of USD 350–450.

These results establish the feasibility of the low-cost architecture but not its reliability or safety for users. The identified design corrections (higher-torque drive, cleated tread, stabilisation and fail-safe braking) must be implemented and verified over a larger number of trials and staircases before any user evaluation.

10.FUTURE WORK

The following specific steps are planned to improve climbing performance and user safety:

- Traction: replace the smooth-rubber tread with a cleated polyurethane tread and verify $\mu_s \geq 0.8$ on concrete, tile and marble nosings (a margin of at least 25% over μ_{req} = 0.64).
- Stability: add a motorized front stabilisation arm or a seat-tilt (CoG-shifting) mechanism, controlled from an IMU, to obtain a positive static stability margin ($\beta \geq 10°$) on the flight and throughout the terminal-step transition without attendant support, verified with the measured centre of gravity.
- Drive torque: replace the direct-drive hub motors with geared hub motors or add a reduction stage so that the continuous torque is at least ≈106 N·m per wheel (the quasi-static demand for the 130 kg design mass), preferably ≈130 N·m for a 25% margin, and add motor current and temperature monitoring.
- Actuation: increase the actuator moment arm d_A to at least 203 mm or use actuators rated at least 565 N (SF ≥ 1.5 at the 130 kg design mass), and provide a stroke of at least 110 mm so that the full 27°–35° pitch range can be reached.
- Fail-safe braking: fit power-off-engaged electromagnetic brakes and verify that the chair holds its position on the 32.5° pitch after an emergency stop at every step.
- Sensing: add downward-facing distance sensors for stair-edge detection (required because the infrared obstacle stop is inhibited in climbing mode) and an IMU-based climbing interlock, and evaluate infrared obstacle detection under varying ambient light.
- Connectivity: add a 4G/LTE module and implement location-aware caregiver alerts triggered by climbing-mode activation or tilt events.
- Validation: repeat the stair trials with at least 59 trials per condition on at least three staircase geometries (riser 150–180 mm, tread 250–300 mm) and loads up to 100 kg, including descent, following ISO 7176-28; then, after institutional ethical approval, conduct supervised trials with wheelchair users.
- Life-cycle assessment: conduct an ISO 14040/14044-compliant LCA with a defined functional unit, system boundary and inventory.

AUTHOR CONTRIBUTIONS

G. A. E.: Conceptualization; Methodology; Formal analysis; Investigation; Data curation; Visualization; Validation; Writing original draft; Writing review and editing; Supervision; Project administration.

N. E.: Practical Work Supervision, Writing original draft.

A.M. B.: Conceptualization; Methodology; Investigation; Writing review and editing; Supervision.

ACKNOWLEDGEMENTS

The authors gratefully acknowledge the support provided by the Faculty of Engineering, Heliopolis University, where the originating graduation project was conceived and executed, and the Mechatronics Engineering Laboratory team for their technical assistance during prototype fabrication. The contributions of the graduation project student team — Abdallah Sayed, Ali Mostafa, Amgad Sabry, Aya Mostafa, Mohamed Reda, and Pierre Bassem — are gratefully acknowledged; their preliminary work helped establish the experimental foundation upon which this scientific analysis is built.

ETHICS STATEMENT

No human participants or clinical patients were involved in the present laboratory prototype evaluation; the occupant was simulated by a 70 kg dead weight. Therefore, formal institutional ethical approval was not required.

CONFLICT OF INTEREST STATEMENT

The authors declare that there are no conflicts of interest, financial or otherwise, associated with this work. The research received no commercial sponsorship, and all findings are reported objectively and independently.

FUNDING STATEMENT

This research was supported by the internal research fund of the Faculty of Engineering, Heliopolis University, Cairo, Egypt, under the undergraduate graduation project supervision programme, which funded component purchases only without any role in the study design, analysis, or publication.

DATA AVAILABILITY STATEMENT

The data supporting the findings of this study are available within the article.

REFERENCES

[1] World Health Organization (2022) Global report on health equity for persons with disabilities. World Health Organization, Geneva.

[2] World Health Organization, United Nations Children's Fund (UNICEF) (2022) Global report on assistive technology. World Health Organization and UNICEF, Geneva.

[3] Tao W, Xu J, Liu T (2017) Electric-powered wheelchair with stair-climbing ability. Int J Adv Robot Syst 14(4). https://doi.org/10.1177/1729881417721436

[4] Borg J, Lindström A, Larsson S (2011) Assistive technology in developing countries: a review from the perspective of the Convention on the Rights of Persons with Disabilities. Prosthet Orthot Int 35:20–29. https://doi.org/10.1177/0309364610389351

[5] Hamza SA, Azouz N, Hammam R, Hendawy M (2025) UX placemaking towards the inclusion of persons with disabilities in public places in Egypt's Greater Cairo Region. Cities 161:105886. https://doi.org/10.1016/j.cities.2025.105886

[6] Lawn MJ, Ishimatsu T (2003) Modeling of a stair-climbing wheelchair mechanism with high single-step capability. IEEE Trans Neural Syst Rehabil Eng 11:323–332.

[7] Morales R, Feliu V, González A, Pintado P (2006) Kinematic model of a new staircase climbing wheelchair and its experimental validation. Int J Robot Res 25:825–841.

[8] Cho Y, Kim KJ, Park J, Seo H, Jung H, Kim B, Park D-I, Ahn J, Park C (2024) Design of stair-climbing electric wheelchair with tri-spoke wheel and supporting leg. IEEE Access 12:31853–31861. https://doi.org/10.1109/ACCESS.2024.3371017

[9] Wellman P, Krovi V, Kumar V, Harwin W (1995) Design of a wheelchair with legs for people with motor disabilities. IEEE Trans Rehabil Eng 3:343–353.

[10] Quaglia G, Franco W, Oderio R (2011) Wheelchair.q, a motorized wheelchair with stair climbing ability. Mech Mach Theory 46:1601–1609. https://doi.org/10.1016/j.mechmachtheory.2011.07.005

[11] Akamisaka A, Nagao K (2024) Transformable quadruped wheelchairs capable of autonomous stair ascent and descent. Sensors 24:3675. https://doi.org/10.3390/s24113675

[12] Sharma B, Pillai BM, Borvorntanajanya K, Suthakorn J (2022) Modeling and design of a stair climbing wheelchair with pose estimation and adjustment. J Intell Robot Syst 106:66. https://doi.org/10.1007/s10846-022-01765-3
[13] Pappalettera A, Reina G, Mantriota G (2024) Design and analysis of tracked stair-climbing robot using innovative suspension system. Robotics 13:45. https://doi.org/10.3390/robotics13030045
[14] Uustal H, Minkel JL (2004) Study of the Independence IBOT 3000 Mobility System: an innovative power mobility device, during use in community environments. Arch Phys Med Rehabil 85:2002–2010.
[15] Pappalettera A, Bottiglione F, Mantriota G, Reina G (2023) Watch the next step: a comprehensive survey of stair-climbing vehicles. Robotics 12:74. https://doi.org/10.3390/robotics12030074
[16] Laffont I et al. (2008) Evaluation of a stair-climbing power wheelchair in 25 people with tetraplegia. Arch Phys Med Rehabil 89:1958–1964.
[17] Gubbi J, Buyya R, Marusic S, Palaniswami M (2013) Internet of Things (IoT): a vision, architectural elements, and future directions. Future Gener Comput Syst 29:1645–1660. https://doi.org/10.1016/j.future.2013.01.010
[18] Simpson RC (2005) Smart wheelchairs: a literature review. J Rehabil Res Dev 42:423–436.
[19] Leaman J, La HM (2017) A comprehensive review of smart wheelchairs: past, present, and future. IEEE Trans Hum-Mach Syst 47:486–499.
[20] Muangmeesri B, Wisaeng K (2022) IoT-based discomfort monitoring and a precise point positioning technique system for smart wheelchairs. Appl Syst Innov 5:103. https://doi.org/10.3390/asi5050103
[21] Gradim LCC, Santana ALM, José MA, Zuffo MK, Lopes RD (2023) An automated electronic system in a motorized wheelchair for telemonitoring: mixed methods study based on Internet of Things. JMIR Form Res 7:e49102. https://doi.org/10.2196/49102
[22] Hashem OA, Bassiuny AM, Hussein HMA, Elgamal GA (2026) Digital twin architectures for remote monitoring and control in CNC manufacturing systems: a systematic review. Evol Intell 19:137. https://doi.org/10.1007/s12065-026-01254-8
[23] Zhu Y, Li H, Lyu S, Shan X, Jan Y-K, Ma F (2023) Stair-climbing wheelchair proven to maintain user's body stability based on AnyBody musculoskeletal model and finite element analysis. PLoS ONE 18:e0279478. https://doi.org/10.1371/journal.pone.0279478
[24] Hojjati Najafabadi A, Amini S, Farahmand F (2021) Improving sit-to-stand transition by the saddle-assistive device in the spinal cord injury: a case study. Proc Inst Mech Eng H 235:735–742. https://doi.org/10.1177/09544119211003370
[25] Hojjati Najafabadi A, Amini S, Farahmand F (2021) Using a saddle-assistive device equipped with mechanical orthosis for walking of the person with incomplete spinal cord injury. Proc Inst Mech Eng H 235:1088–1095. https://doi.org/10.1177/09544119211020146
[26] Hojjati Najafabadi A, Amini S, Farahmand F (2020) The effect of saddle-assistive device on improving the gait parameters of patients with the lower limbs weakness: a pilot study. J Bionic Eng 17:1175–1185. https://doi.org/10.1007/s42235-020-0088-2
[27] Hojjati Najafabadi A, Ahmadi Bani M, Pourmoghadam V (2022) Comparison of anterior and posterior wheeled walkers based on body weight support in improving gait function a subjects with spinal cord injury: a case study. Proc Inst Mech Eng H 236:1366–1372. https://doi.org/10.1177/09544119221131882
[28] Elgamal GA, Elazab R, Abdelkader AM (2026) Human-Centered Smart Safety Sustainability Index (HS3I): a novel framework for evaluating human safety in intelligent automated vehicles. Sustainability 18:8867. https://doi.org/10.3390/su18178867
[29] International Electrotechnical Commission (2016) IEC 60204-1:2016 Safety of machinery — Electrical equipment of machines — Part 1: General requirements. IEC, Geneva.
[30] Padhi AK, Nanjundaswamy KS, Goodenough JB (1997) Phospho-olivines as positive-electrode materials for rechargeable lithium batteries. J Electrochem Soc 144:1188–1194. https://doi.org/10.1149/1.1837571
[31] Nitta N, Wu F, Lee JT, Yushin G (2015) Li-ion battery materials: present and future. Mater Today 18:252–264. https://doi.org/10.1016/j.mattod.2014.10.040
[32] u-blox AG (2011) NEO-6 u-blox 6 GPS modules data sheet (GPS.G6-HW-09005). u-blox, Thalwil.
[33] Blau PJ (2008) Friction science and technology: from concepts to applications. 2nd edn. CRC Press, Boca Raton.
[34] International Organization for Standardization (2014) ISO 7176-1:2014 Wheelchairs — Part 1: Determination of static stability. ISO, Geneva.
[35] International Organization for Standardization (2012) ISO 7176-28:2012 Wheelchairs — Part 28: Requirements and test methods for stair-climbing devices. ISO, Geneva.
[36] Clopper CJ, Pearson ES (1934) The use of confidence or fiducial limits illustrated in the case of the binomial. Biometrika 26:404–413. https://doi.org/10.1093/biomet/26.4.404
[37] El Gamal GA, Gomaa AM, Daowd M (2024) Circular economy in engineering education: enhancing quality through project-based learning and assessment. Adv Sci Technol J 1:1–17. https://doi.org/10.21608/astj.2024.345935.1032